

# Illumination Invariant Measurement of Mechanical Dimensions Using a Multiple Segmentation Method

Kevin Ohliger, Torsten Edeler, and Stephan Hussmann  
Department of Electrical Engineering and Information Technology  
Westcoast University of Applied Sciences  
25746 Heide, Germany  
Email: ohliger@fh-westkueste.de

Alfred Mertins (IEEE Senior Member)  
Institute for Signal Processing  
University of Lübeck  
23538 Lübeck, Germany

**Abstract**—In many industrial processes the need for better quality assurance leads to a higher degree of process automation which often includes an optical inspection system. In our case the mechanical dimensions of printed micro structures on ceramic substrates have to be evaluated. Therefore an optical inspection system providing high resolution images with 12288 pixel x 14000 pixel was developed. The segmentation task in this setup is challenging caused by the huge amount of data and the different appearances of the micro structures depending on size, material, and humidity. For this purpose we present a multiple segmentation method and evaluate the results against common used segmentation methods on a number of different real images. Experimental results show that the proposed optical inspection system and algorithms can achieve an illumination invariant high resolution measurement of the micro structures.

**Index Terms**—high resolution, optical inspection system, maximally stable extremal regions, MSER, adapted maximally stable extremal regions, AMSER, segmentation, illumination invariant, region of interest, ROI

## I. INTRODUCTION

The production of passive electronic devices such as chip resistors has the need of high throughput in order to generate profit. The processes are sometimes not optimally configured and thus lots of rejects and therefore higher production costs are produced. In order to keep the costs low the invalid products have to be excluded from the production process as soon as possible. In this paper we present an optical inspection system for evaluating the print process in the chip resistor production.

An optical inspection system for measuring mechanical dimensions can be divided into three main parts:

- 1) image acquisition
- 2) image improvement
- 3) image and data analysis

Section II describes briefly the image acquisition focussing on the hardware design of the system including the selection and formation of the hardware. Image improvement concentrates on image enhancement and restauration [1]. This is not a topic of this work. Interpreting the content of the image

is done in the image analysis part containing methods for feature extraction, segmentation, detection, and registration. The image and data analysis for a single inspection task which is focussed on segmentation, is described in Section III, where the proposed approach is presented.

Due to the various objectives of inspection systems the topics mentioned for image improvement and analysis are still focussed by actual research [2], [3], [4], [5]. Segmentation is mostly based on amplitude, clustering, region, edge or texture segmentation methods. Caused by high variance of the surface structure (from homogeneous to heterogeneous reflectance behavior) and varying illumination, simple segmentation methods are not applicable in our case. Evaluations in literature [6], [7], [8] show that maximally stable extremal regions and watershed methods for segmentation lead to good results in the respective test cases. Our approach for segmentation is a novel multiple segmentation method based on adapted maximally stable extremal regions and analytical segmentation approaches. Our Method is focussed on decreasing false-positive errors in comparison to single segmentation methods while considering a few assumptions. Experimental results are presented in Section IV and Section V introduces a measurement model for determining the uncertainty of the measurement system. Conclusion remarks are made in the last section.

## II. HARDWARE SETUP AND REQUIREMENTS

Our proposed optical inspection system was designed for measuring mechanical dimensions of printed structures on ceramic substrates. These substrates have the dimension of 5cm x 6cm and the printed structures can scale down to less than 50 microns. A monochrome line scan camera with 12288 pixels combined with a lens of 0.7 magnification and a linear motion transport system leads to a spatial resolution of 6.5 $\mu$ m in both directions. In order to adapt to multiple inspection tasks a front and background illumination are installed. The processing unit is a standard PC with additional framegrabber and I/O card as shown in Fig. 1.

## III. PROPOSED APPROACH

In Fig. 2 a blockdiagram of the segmentation algorithm is shown. In this section we first describe our illumination

<sup>0</sup>This project is sponsored by the European Union (EFRE) and the federal state of Schleswig-Holstein, Germany (Zukunftsprogramm Wirtschaft)



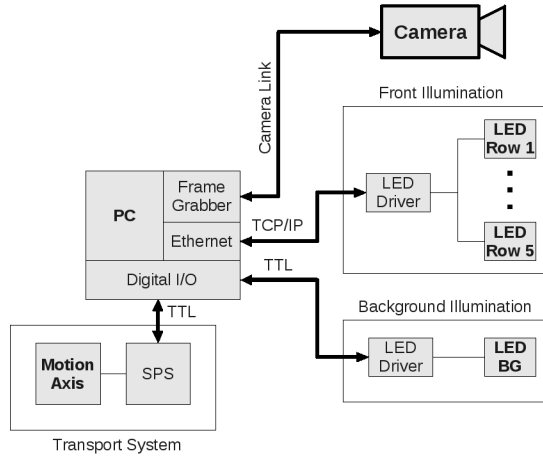


Fig. 1. Schematic Overview of the Inspection System

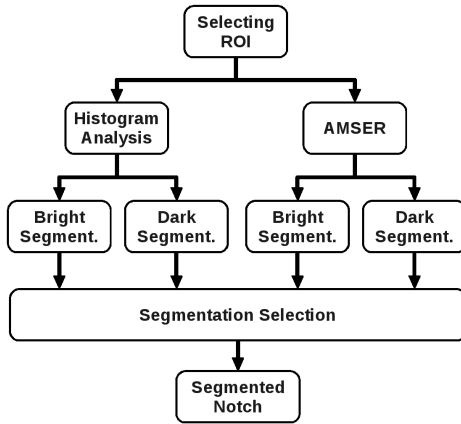


Fig. 2. Blockdiagram of the Segmentation Algorithm

invariant approach for finding region of interests (ROIs) and our solution for segmentation of horizontal notches.

#### A. Finding Region of Interests

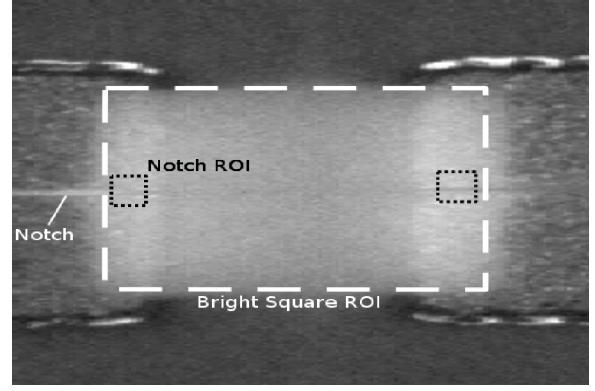
In order to reduce computational costs and increase stability of analyzing locally varying images it is common to analyze only a subset of the image called regions of interests. For finding the ROIs we use a global illumination invariant segmentation method and prior knowledge.

[2] introduced the reflection model for the sensor output

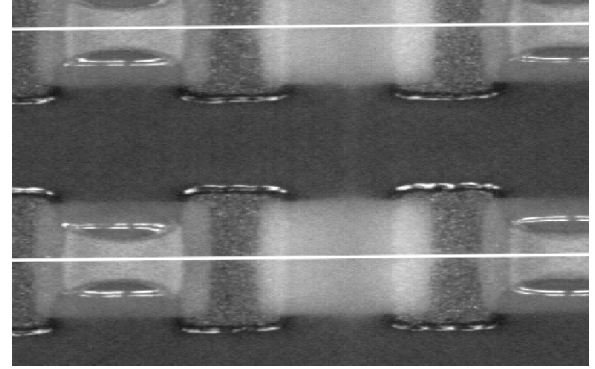
$$\rho(\mathbf{x}) = \int_{\lambda_{min}}^{\lambda_{max}} E(\mathbf{x}, \lambda) L(\mathbf{x}, \lambda) F(\lambda) d\lambda, \quad (1)$$

while  $\lambda_{min}$ ,  $\lambda_{max}$  are the limits of the spectral sensitivity  $F(\lambda)$  of the camera including the optics.  $E(\mathbf{x}, \lambda)$  is the spectral power distribution of the incident light and  $L(\mathbf{x}, \lambda)$  describes the spectral reflection behavior caused by the material and surface structure at location  $\mathbf{x}$ . We assume that our image contains  $N$  different regions  $\mathcal{R}_i$  with uniform reflection behavior inside these regions:

$$L(\mathbf{x} \in \mathcal{R}_i, \lambda) = L_i(\lambda), \quad (2)$$



(a)



(b)

Fig. 3. Distance Measuring Between the Horizontal Notches  
(a) White Square: ROI of Bright Square, Black Squares: ROIs of Notches  
(b) White Lines: Reference Notch Lines

while  $i = 1, \dots, N$ . Assuming that the spectral power distribution of the incident light in our scene is homogeneous

$$E(\mathbf{x}, \lambda) = E(\lambda) \quad (3)$$

and in our illumination setup we expect  $E(\lambda)$  to be time variant

$$\forall_{t_0} \exists \Delta t : E(\lambda, t_0) \neq E(\lambda, t_0 + \Delta t) \quad (4)$$

This is caused by temperature drift and aging of the illumination source. Further we assume that the relative spectral power distribution

$$E_{rel}(\lambda, t) = \frac{E(\lambda, t)}{\int_{\lambda_{min}}^{\lambda_{max}} E(\lambda, t) d\lambda} = \frac{E(\lambda, t)}{E_{tot}(t)} \quad (5)$$

is not affected by these influences:

$$E_{rel}(\lambda, t_0) = E_{rel}(\lambda, t) \quad (6)$$

This leads to the relationship

$$E(\lambda, t) = \frac{E_{tot}(t)}{E_{tot}(t_0)} \cdot E(\lambda, t_0) = k(t) \cdot E(\lambda, t_0) \quad (7)$$

and with respect to (4) and inserting (7), (2) in (1) the sensor output depending on time can be expressed as

$$\rho(\mathbf{x} \in \mathcal{R}_i, t) = k(t) \int_{\lambda_{min}}^{\lambda_{max}} E(\lambda, t_0) L_i(\lambda) F(\lambda) d\lambda \quad (8)$$

The sensor output is proportional to the intensity image

$$\rho(\mathbf{x}, t) \propto I(\mathbf{x}, t) \quad (9)$$

It is obvious that a variation of illumination leads to a scaling of the intensity values. We chose a global threshold segmentation method with thresholds derived from characteristic histogram properties which are unaffected by scaling of the intensity values. In our case these properties are local minima extracted from the histogram at intensity values  $T_l$  and  $T_h$ . These local minima bound a maxima,  $T_h$  in upward direction and  $T_l$  in downward direction. In the respective maxima we expect the intensity values of the object to be segmented. The segmentation can be expressed as

$$B_{\mathcal{R}}(\mathbf{x}, T_l, T_h) = \begin{cases} 1 & T_l \leq I(\mathbf{x}) < T_h \\ 0 & \text{otherwise} \end{cases} \quad (10a)$$

$$(10b)$$

The dark horizontal stripes shown in Fig. 3b are expected to be located in the first maxima thus  $T_l$  is omitted:

$$B_{\mathcal{R}_1}(\mathbf{x}, T_{h,1}) = \begin{cases} 1 & I(\mathbf{x}) < T_{h,1} \\ 0 & \text{otherwise} \end{cases}, \quad (11a)$$

$$(11b)$$

while  $T_{h,1}$  is the threshold containing the value of the upper bounding minima of the first maximum.  $B_{\mathcal{R}_1}(\mathbf{x}) = 1$  indicates that the pixel at  $\mathbf{x}$  is a member of region  $\mathcal{R}_1$ .

The segmentation of the area exemplarily bounded by the white box in Fig. 3a includes also analyzing of the histogram. We use the prior knowledge that this area, named bright squares, has the brightest elements except of some total reflectance points. We also know that the total area of the bright squares is less than 20 percent of the image area. Thus we use the lower threshold  $T_l = T_{80\%}$  and a higher threshold is not applicable:

$$B_{\mathcal{R}_2}(\mathbf{x}, T_{80\%}) = \begin{cases} 1 & I(\mathbf{x}) > T_{80\%} \\ 0 & \text{otherwise} \end{cases} \quad (12a)$$

$$(12b)$$

The binary image  $B_{\mathcal{R}_2}(\mathbf{x})$  includes  $K$  connected regions  $\mathcal{R}_{2,k}$  with  $k = 1 \dots K$  containing the squares but also total reflectance points which are assumed to be smaller than the squares. Excluding the latter with

$$\tilde{\mathcal{R}}_{2,k} = \begin{cases} \mathcal{R}_{2,k} & A(\mathcal{R}_{2,k}) \geq A_{\min} \\ \emptyset & \text{otherwise} \end{cases}, \quad (13a)$$

$$(13b)$$

while  $A(\mathcal{R}_{2,k})$  is the area of  $\mathcal{R}_{2,k}$  and  $A_{\min}$  is the minimum area of the bright squares.

### B. Segmentation of Horizontal Notches

The measurement of the distance between notches is done by determining the distance between the white lines shown in Fig. 3b. These lines are generated by interpolating the segmented notches region points. As shown in Fig. 3a the notches sometimes appear brighter and sometimes darker than the background. The dark rectangles indicate the ROIs for the segmentation of the horizontal notches. These ROIs are directly derived from the ROIs of the bright squares.

Fig. 2 shows the segmentation algorithm for the horizontal notches. The histogram analysis segmentation, AMSER and segmentation selection are described below.

1) *Histogram Analysis Segmentation*: We assume that that notches appearing bright are leading to a maximum next to  $I_{max}$ , the segmentation is done by using (10).  $I_{max}$  is the maximum and  $I_{min}$  the minimum intensity value of  $I(\mathbf{x})$ .  $T_{l,3}$  is the respective minimum and  $T_{h,3} = I_{max}$  and thus is omitted:

$$B_{\mathcal{R}_3}(\mathbf{x}, T_{l,3}) = \begin{cases} 1 & I(\mathbf{x}) \geq T_{l,3} \\ 0 & \text{otherwise} \end{cases} \quad (14a)$$

$$(14b)$$

In addition to (14) a segmentation analogue to the method described in Section III-A by using (12) with an adapted threshold

$$B_{\mathcal{R}_4}(\mathbf{x}, T_{95\%}) = \begin{cases} 1 & I(\mathbf{x}) \geq T_{95\%} \\ 0 & \text{otherwise} \end{cases} \quad (15a)$$

$$(15b)$$

For dark appearance of notches equations (14) and (15) can be easily adapted.

2) *AMSER Segmentation*: For segmentation of different elements in the respective ROI we modify the maximally stable extremal region (MSER) approach to the adapted maximally stable extremal region (AMSER) method. In order to find the MSER threshold for a connected black ( $B_{\mathcal{R}_i}(\mathbf{x}) = 0$ ) region  $\mathcal{R}_i$  the initial threshold  $T_l = T_0$  is increased to  $T_h = T_j$  as long as the area change

$$\Delta A_{\mathcal{R}_i, T_j, T_0} = \frac{A(\mathcal{R}_i(T_j)) - A(\mathcal{R}_i(T_0))}{A\left(\mathcal{R}_i\left(\frac{T_0+T_j}{2}\right)\right)} \quad (16)$$

is smaller than the maximum area change  $\Delta A_m$ . If this is not fulfilled and the difference  $\Delta T$  between  $T_j$  and  $T_0$  is larger than the minimum margin  $M$  the regions  $\mathcal{R}_i(T_{j-1})$  and  $\mathcal{R}_i(T_0)$  are called extremal regions of  $\mathcal{R}_i$ . In order to use the MSER for connected white regions  $T_h$  is hold on its initial value and  $T_l$  is decreased and the segmented regions can be expressed as

$$\tilde{\mathcal{R}}_i = \begin{cases} \mathcal{R}_i(T_{j-1}) & (\Delta A_{\mathcal{R}_i, T_j, T_0} < \Delta A_m) \wedge (\Delta T > M) \\ \emptyset & \text{otherwise} \end{cases} \quad (17a)$$

$$(17b)$$

A more detailed description of MSER is given in [6], [7], [8]. In our case we assume that the horizontal notches regions are either located at the lower bound or higher bound of the histogram. Thus  $T_l = I_{min}$  for dark notches and  $T_h = I_{max}$  for bright ones. We select the minimum margin  $M = 0$  caused by the consideration that for an illumination invariant algorithm the notch intensities could be completely at the boundaries of the histogram. This would lead for  $M > 0$  to no maximum stable extremal regions and thus the notches would not be segmented. (17) changes for dark notches to

$$\tilde{\mathcal{R}}_i = \begin{cases} \mathcal{R}_i(T_{j-1}) & \Delta A_{\mathcal{R}_i, T_j, 0} < \Delta A_m \\ \emptyset & \text{otherwise} \end{cases} \quad (18a)$$

$$(18b)$$

and for bright notches

$$\tilde{\mathcal{R}}_i = \begin{cases} \mathcal{R}_i(T_{j-1}) & \Delta A_{\mathcal{R}_i, T_h, T_j} < \Delta A_m \\ \emptyset & \text{otherwise} \end{cases}, \quad (19a)$$

$$(19b)$$

while  $\Delta A_m$  is chosen to be 2.5 percent of the total ROI area.

3) *Segmentation Selection*: As shown in Fig. 2 the segmentation methods described in the previous Sections III-B1 and III-B2 can result in more than one segmentation for each ROI. Thus we propose an analyzing module for selecting the most appropriate segmentation. Given  $K$  segmented regions  $R_k$  with  $k = 1, \dots, K$  the region count is reduced by

$$\tilde{\mathcal{R}}_i = \begin{cases} \mathcal{R}_i & (W_i > W_m) \wedge (A_i < A_m) \wedge (|\phi_i| < |\phi|_m) \\ \emptyset & \text{otherwise} \end{cases}, \quad (20a)$$

while  $W_i$  is the width,  $A_i$  the area, and  $\phi_i$  the orientation of  $\mathcal{R}_i$ .  $W_m = 3px$  is the minimal width and  $A_m = A_{ROI}/3$  is the maximal expected area of the notch region.  $|\phi|_m$  describes an orientation range of the smallest bounding rectangle including the respective region. This ensures that the detected region has approximately the same orientation as the expected notches. We assume that the horizontal notches have an orientation of  $|\phi| < 0.4rad$ . If (20) returns more than one region for a ROI then all regions are rejected.

#### IV. EXPERIMENTAL RESULTS

This section evaluates the multiple segmentation method described in Section III-B against the single methods within invariant and variant illumination settings.

1) *Invariant Illumination Setup*: The evaluation of the proposed method for the horizontal notches segmentation includes the analyzing of 80 ROIs taken from the same image. The analytical segmentation, the AMSER and the segmentation selection module are evaluated each for themselves and in combination. Therefore we define the relative class error 1  $\epsilon_1$  and relative class error 2  $\epsilon_2$  as

$$\epsilon_1 = \frac{s_{bg}}{n_{bg}}; \quad \epsilon_2 = \frac{s_{fg}}{n_{fg}}, \quad (21)$$

while  $\epsilon_1$  includes the ratio between segmented background pixel  $s_{bg}$  and total count of background pixel  $n_{bg}$  and  $\epsilon_2$  analogue for foreground.  $\epsilon_1$  is a relative false-positive error criterion.  $n_\emptyset$  contains the count of ROIs where  $s_{fg} = s_{bg} = 0$ . The mean  $\mu$  and standard deviation  $\sigma$  are calculated on the distance of the interpolated lines to the real notches. The sample set includes ten notches. The results are shown in TABLE I.

It is obvious that combining of all methods leads to the best results for  $\epsilon_1$  and the statistical parameters of the measured values. The omitting of the selection module leads to less  $n_\emptyset$  and lower  $\epsilon_2$  but also to a strong increase of  $\epsilon_1$ . The performance of the AMSER segmentation method is poor but nevertheless in combination with the other methods it decreases both errors and the standard deviation of the distance measurement.

2) *Variant Illumination Setup*: In TABLE II are the segmentation error rates and statistic parameters of the distance measurement for four images which were taken from four different scenes with different illuminations. The proposed segmentation method combining all methods described above was used. Fig. 4 shows the varying histograms of the images. The sample set consists of 80 ROIs and ten reference notches.

TABLE I  
EVALUATION OF SEGMENTATION METHODS IN AN ILLUMINATION INVARIANT SETUP

Method	$\epsilon_1$	$\epsilon_2$	$n_\emptyset$	$\mu[\mu m]$	$\sigma[\mu m]$
All Combined	0	7.7e-1	15	2.5	3.4
All Combined without Selection Mod.	1.2e-1	6.9e-1	1	12.7	5.2
AMSER with Selection Mod.	4.8e-3	9.1e-1	66	382.0	570.1
Analytical Seg. with Selection Mod.	1.0e-4	8.0e-1	21	2.5	4.1

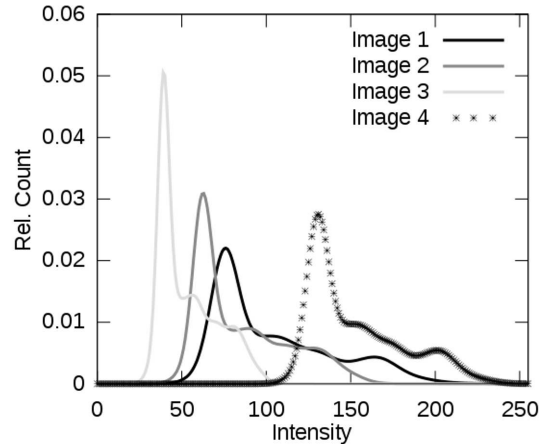


Fig. 4. Histograms of the Different Images

TABLE II  
EVALUATION OF SEGMENTATION METHODS IN AN ILLUMINATION INVARIANT SETUP

Image No.	$\epsilon_1$	$\epsilon_2$	$n_\emptyset$	$\mu[\mu m]$	$\sigma[\mu m]$
1	0	7.76e-1	15	2.5	3.4
2	0	6.9e-1	2	1.5	2.3
3	0	7.1e-1	3	1.5	2.3
4	0	7.6e-1	9	3.1	2.5

The mean values of the distances between the reference notches and the detected notches vary from  $1.5\mu m$  to  $3.1\mu m$  and the standard deviations are less than  $3.4\mu m$ . The relative class 1 error is for all illumination settings zero. The variation of  $\epsilon_2$  and the standard deviation are maximal between the segmentations of image 1 and image 2 which have similar histograms but different image context. Although the mean of the histograms and therefore the illumination of image 2, 3 and 4 differ significantly the variations are smaller than in the first case. Thus for the evaluated images the segmentation and measurement errors vary more influenced by the image context than by illumination changes. This indicates that our segmentation method is within the tested boundaries illumination invariant.

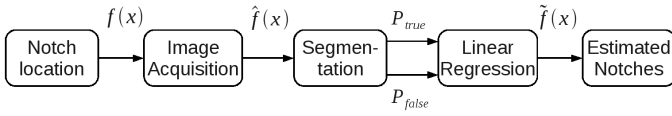


Fig. 5. Blockdiagram of the measurement model

## V. MEASUREMENT UNCERTAINTY

This section introduces a model for the measurement process in order to characterize the measuring system. As introduced in [9], [10] the measurement uncertainty expresses the degree of belief based on probabilities. In this section we concentrate on the random errors assuming that the systematic errors are compensated within the calibration of the measurement system which is not topic of this work. In Fig. 5 the multistage measurement model is shown. The input of the measurement model are the notch locations and can be described for every notch with a linear equation

$$f(x) = m \cdot x + c, \quad (22)$$

while  $x$  is the respective horizontal position,  $m$  the gradient,  $c$  the offset and  $f(x)$  is the vertical position. Caused by the horizontal direction of the notches  $m$  is assumed to be  $[-1, 1]$ . This information is forwarded to the image acquisition. The output generates degraded notch positions  $\hat{f}(x)$  with an uncertainty of  $\sigma_{\hat{f}} \approx 10\mu m$  determined by previous calibration of the measurement system. These positions are passed to the segmentation algorithms described in Section III. The output can be parted into segmented notch points  $P_{\text{true}}$  and segmented background points (class error 1 as described in Section IV)  $P_{\text{false}}$ . The distribution of the vertical component  $y_{\text{true}}$  and horizontal component  $x_{\text{true}}$  of  $P_{\text{true}}$  is given by

$$y_{\text{true}}(x) \sim \mathcal{N}(f(x), \sigma_{\hat{f}}) \quad (23)$$

and

$$x_{\text{true}}(x) \sim \mathcal{N}(x, \sigma_{\hat{f}}) \quad (24)$$

derived from the uncertainty resulting from the image acquisition process. The distribution of the vertical component  $y_{\text{false}}$  and  $x_{\text{false}}$  of  $P_{\text{false}}$  is assumed to be uniformly distributed bounded by the borders of the ROI and excluding the region of the notch locations described with equations (23) and (24). This results in the distribution function

$$g_y(y'; x) = \begin{cases} k_y & y' > f(x) + \sigma_{\hat{f}} \vee y' < f(x) - \sigma_{\hat{f}} \\ 0 & \text{otherwise} \end{cases} \quad (25a)$$

$$(25b)$$

for  $y_{\text{false}}$  and

$$g_x(x'; x) = \begin{cases} k_x & x' > x + \sigma_{\hat{f}} \vee x' < x - \sigma_{\hat{f}} \\ 0 & \text{otherwise} \end{cases} \quad (26a)$$

$$(26b)$$

for  $x_{\text{false}}$  with the normalization constants

$$k_y = \frac{1}{H_{\text{ROI}} - 2\sigma_{\hat{f}}} \quad \text{and} \quad k_x = \frac{1}{W_{\text{ROI}} - 2\sigma_{\hat{f}}} \quad (27)$$

including the height  $H_{\text{ROI}}$  and width  $W_{\text{ROI}}$  of the ROI. In our case the ROI is expected to be square resulting in

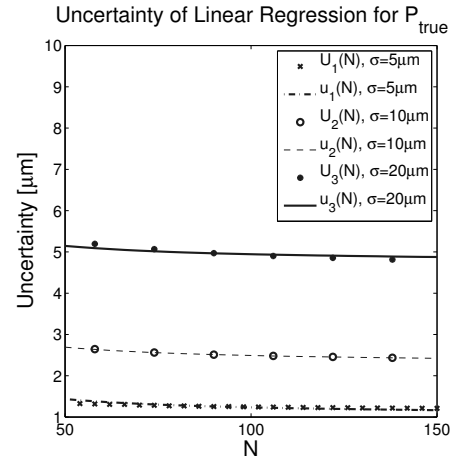


Fig. 6. Uncertainty resulting from linear regression using  $P_{\text{true}}$ .  $U$  shows the statistically determined uncertainty values and  $u$  the estimated function of  $U$ .

$k_y = k_x$ . Both  $P_{\text{true}}$  and  $P_{\text{false}}$  are used to perform a linear regression for estimating the linear equation describing the notch locations

$$\tilde{f}(x) = \tilde{m} \cdot x + \tilde{c}. \quad (28)$$

The estimation of  $\tilde{m}$  and  $\tilde{c}$  by means of the linear regression depending on  $P_{\text{true}}$  and  $P_{\text{false}}$  is described by

$$\tilde{m} = \frac{\sum_{i=1}^N (x_i - \bar{x})(y_i - \bar{y})}{\sum_{i=1}^N (x_i - \bar{x})^2} \quad (29)$$

and

$$\tilde{c} = \bar{y} - \tilde{m} \cdot \bar{x}, \quad (30)$$

while  $N$  is the total count of segmented notches,  $\bar{x}$  the mean of  $x$ ,  $\bar{y}$  the mean of  $y$ ,  $x_i$  and  $y_i$  are the coordinate components of segmented point  $i$ . For describing the measurement uncertainty resulting in  $\tilde{f}(x)$  the Monte Carlo method described in [9], [10] was used. The resulting function for  $P_{\text{true}}$  is shown in Fig. 6. and for  $P_{\text{false}}$  in Fig. 7. The estimated function  $u$  depends on the uncertainty  $\sigma_{\hat{f}}$  and the total count of segmented points  $N$

$$u(N, \sigma_{\hat{f}}) = 91.49\mu m \cdot e^{-9.1 \cdot 10^{-6} \cdot N} + 1.15\mu m \cdot e^{-0.036 \cdot N} + \sigma_{\hat{f}} \cdot 0.25 - 91.46\mu m \quad (31)$$

and shows in the relevant intervals

$$\sigma_{\hat{f}} = [5\mu m, 20\mu m] \quad (32)$$

and

$$N = [50, 150] \quad (33)$$

low deviations to the statistical determined uncertainty  $U$ . The estimated function  $v$  depends on the Height of the ROI  $H_{\text{ROI}}$  and the total count of segmented points  $N$

$$v(N, H_{\text{ROI}}) = 4.23\mu m \cdot e^{-1.10 \cdot 10^{-4} \cdot N} + 1.27\mu m \cdot e^{-1.44 \cdot 10^{-2} \cdot N} + H_{\text{ROI}} \cdot 0.135 - 2.01\mu m \quad (34)$$

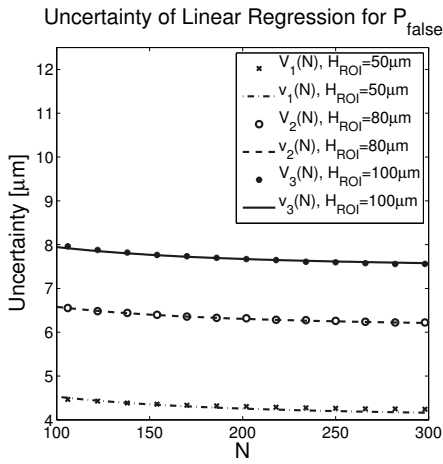


Fig. 7. Uncertainty resulting from linear regression using  $P_{\text{false}}$ .  $V$  shows the statistically determined uncertainty values and  $v$  the estimated function of  $V$ .

TABLE III  
MEASUREMENT UNCERTAINTY IN AN ILLUMINATION INVARIANT SETUP

Id	Method	$\bar{N}_{\text{true}}$	$\bar{N}_{\text{false}}$	$w(\Theta)$ [ $\mu\text{m}$ ]
1	All Combined	109	0	2.5
2	All Combined without Selection Mod.	153	341	5.0
3	AMSER with Selection Mod.	100	3	2.7
4	Analytical Seg. with Selection Mod.	50	14	3.7

and shows in the relevant intervals

$$H_{\text{ROI}} = [50\mu\text{m}, 100\mu\text{m}] \quad (35)$$

and

$$N = [100, 300] \quad (36)$$

low deviations to the statistical determined uncertainty  $V$ . Both uncertainty functions  $u$  and  $v$  were determined by forwarding only  $P_{\text{true}}$  and  $P_{\text{false}}$  separately to the linear regression process. If both components are passed to the process the combined uncertainty function is expected to be

$$w(\Theta) = \frac{\Theta_2 \cdot u(\Theta_1, \Theta_2) + \Theta_4 \cdot w(\Theta_3, \Theta_4)}{\Theta_2 + \Theta_4} \quad (37)$$

with

$$\Theta = [\Theta_1, \Theta_2, \Theta_3, \Theta_4] = [\sigma_{\hat{f}}, N_{\text{true}}, H_{\text{ROI}}, N_{\text{false}}] \quad (38)$$

while  $N_{\text{true}}$  is the total count of  $P_{\text{true}}$  and  $N_{\text{false}}$  for  $P_{\text{false}}$ . The results of the measurement uncertainty calculation are shown in TABLE III.  $\bar{N}_{\text{true}}$  and  $\bar{N}_{\text{false}}$  are the mean values of the respective counts of segmentation points. The mean width and height of the ROI was determined to be 80 microns in all cases. The differences between the evaluated uncertainty shown in TABLE I and the estimated uncertainty listed in

TABLE III are for methods 1, 2, and 4 less than 0.9 microns although the intervals given in equations (33) and (36) have been weakly exceeded. The uncertainty determined for method 3 differs significantly from the evaluated uncertainty. This indicates that the measurement model developed in this section does not fit to method 3. This can be caused by disregarding  $n_0$  or inhomogeneous distribution of segmentation points over the ROIs.

## VI. CONCLUSION

Experimental results show that the proposed hardware setup and the illumination invariant multiple segmentation method lead to an optical inspection system which is able to measure the position of notches with a mean measurement error of less than 3.1 microns and a standard deviation of less than 3.4 microns in an illumination variant environment. It is shown that the influence of the scene variation on the measurement results are higher than the variation of the illumination. The uncertainty of the measurement system determined by the introduced measurement model shows only small differences of less than 0.9 microns to the experimental results for the preferred segmentation methods.

In order to improve the segmentation results the adapted maximally stable extremal regions segmentation method and a more appropriate segmentation selection algorithm have to be investigated. Future work will also concentrate on evaluation of our approach with more samples in different illumination settings.

## REFERENCES

- [1] W. K. Pratt, *Digital Image Processing*. New York, USA: JOHN WILEY & SONS, INC., 1991.
- [2] T. Gevers and A. Smeulders, "Pictoseek: combining color and shape invariant features for imageretrieval," *IEEE Trans. Image Process.*, vol. 9, no. 1, pp. 102–119, 2000.
- [3] R. Alferez and Y. Wang, "Geometric and illumination invariants for object recognition," *IEEE Trans. Pattern Anal. Mach. Intell.*, vol. 21, no. 6, 1999.
- [4] G. Healey and D. Slater, "Computing illumination-invariant descriptors of spatially filtered color image regions," *IEEE Trans. Image Process.*, vol. 6, no. 7, pp. 1002–1013, 1997.
- [5] D. Toth, T. Aach, and V. Metzler, "Illumination-invariant change detection," in *Proc. IEEE SSIAI 00*, 2000, pp. 3–7.
- [6] L. Shafarenko, M. Petrou, and J. Kittler, "Automatic watershed segmentation of randomly textured color images," *IEEE Trans. Image Process.*, vol. 6, no. 11, pp. 1530–1544, 1997.
- [7] J. Matas, O. Chum, M. Urban, and T. Pajdla, "Robust wide baseline stereo from maximally stable extremal regions," in *Proc. 13th British Machine Vision Conf. 02*, 2002, pp. 384–393.
- [8] F. Fraundorfer and H. Bischof, "A novel performance evaluation method of local detectors on non-planar scenes," in *Computer Vision and Pattern Recognition - Workshops, 2005. CVPR Workshops*, Nagoya, Japan, Jun. 2005.
- [9] J. C. for Guides in Metrology, *Evaluation of measurement data - An introduction to the Guide to the expression of uncertainty in measurement and related documents*. Geneva, Switzerland: Joint Committee for Guides in Metrology, 2009.
- [10] BIPM, IEC, IFCC, ISO, IUPAC, IUPAP, and OIML, *Uncertainty of measurement - Part 3: Guide to the expression of uncertainty in measurement (GUM:1995)*. Geneva, Switzerland: ISO/IEC, 2008.